Draft version October 10, 2012
Preprint typeset using LaTeX style emulateapj v. 5/2/11

arXiv:1210.2469v1 [astro-ph.HE] 9 Oct 2012

THE BENEFITS OF VLBI ASTROMETRY TO PULSAR TIMING ARRAY SEARCHES FOR GRAVITATIONAL RADIATION

D.R. Madison[1], S. Chatterjee[2], and J.M. Cordes[2]
Cornell University, Ithaca, NY 14853

Draft version October 10, 2012

ABSTRACT

Precisely measured astrometric parameters are integral to successful pulsar timing campaigns. They are commonly measured by fitting the astrometric parameters of a deterministic timing model to a series of pulse times of arrival (TOAs). TOAs measured to microsecond precision over several-year spans can in this way provide astrometric parameters precise to sub-milliarcsecond levels. However, pulsars do not pulsate in a deterministic fashion. Many display significant amounts of red spin noise. Furthermore, a stochastic background of gravitational waves can lead to red noise-like structure in TOAs. We investigate how noise of different spectral types is absorbed by timing models and leads to significant estimation errors in the astrometric parameters. Independent of timing, very long baseline interferometry (VLBI) is capable of providing sub-milliarcsecond astrometric parameters for pulsars. We find that incorporating VLBI astrometric measurements into the timing models of pulsars for which only a couple of years of timing data exist will lead to more realistic assessments of red spin noise, yield more accurate astrometric parameters, and could enhance the amplitude of certain gravitational wave signatures in post-fit timing residuals by factors of 20 or more.

Subject headings: astrometry – gravitational waves – pulsars: general – reference systems

1. INTRODUCTION

Successfully timing a pulsar relies on the extraordinarily stable evolution of the rotational phase of that pulsar and the fact that its phase can be tracked as it beams pulses of light towards Earth at nearly fixed points in its phase. The pulses traveling towards Earth leave the pulsar at intervals indicating the phase evolution of the pulsar, but those intervals are modulated before reaching Earth by many astrophysical processes. To regain the phase information of the pulsar, one must develop a detailed mathematical model (a timing model) that accounts for all the deterministic physical effects that cause pulses to arrive at Earth at intervals differing from those with which they were emitted. The main data products of a pulsar timing campaign are a set of parameters describing the astrophysical phenomena being modeled and a series of timing residuals—the differences between measured pulse arrival times and the predictions of the timing model. A successful timing model paired with a pulsar rotating in a predictable way will yield timing residuals consistent with white noise (Manchester & Taylor 1977; Blandford et al. 1984; Lorimer & Kramer 2005).

The precise astrometric parameters of a pulsar (right ascension and declination $(\alpha, \delta) \equiv \boldsymbol{\theta}$, proper motion $(\mu_\alpha, \mu_\delta) \equiv \boldsymbol{\mu}$, and parallax π) are essential to successful timing models. An error in position of just a tenth of an arcsecond can lead to annual oscillations in residuals of over 100 μs in amplitude (see Figure 1). With software like TEMPO2 (Hobbs et al. 2006), timing models are refined through least squares fitting to minimize the amplitude of such signatures in the residuals. For a particularly stable subset of recycled (millisecond) pulsars (MSPs), measuring pulse times of arrival (TOAs) with microsecond precision or better and refining the timing model parameters to minimize the RMS of the residuals can yield sub-milliarcsecond astrometry (Splaver et al. 2005; Hotan et al. 2006; Verbiest et al. 2008). Precise astrometric measurements are also useful in studies of the Galactic neutron star (NS) population (Cordes & Chernoff 1997; Toscano et al. 1999; Faucher-Giguere & Kaspi 2007), NS electromagnetic emission mechanisms (Deller et al. 2009b), the Galactic distribution of interstellar gas (Cordes & Lazio 2002), and the evolution of compact binaries containing pulsars, specifically to correct for the Shklovskii effect (Shklovskii 1969; Deller et al. 2008).

As pulsars are point-like radio sources, their astrometric parameters can also be obtained with very long baseline interferometry (VLBI). VLBI is currently capable of sub-milliarcsecond astrometric measurements of pulsars on par with the best timing-based results. Additionally, VLBI astrometry can arrive at precisions requiring approximately five years of timing data in less than two years (e.g., Chatterjee et al. 2009). To enhance the observation signal-to-noise ratio (S/N), pulsar gating (gathering signal only when the pulsar is beamed towards Earth) is used. The Very Long Baseline Array (VLBA) allows for full-time VLBI and better-controlled systematics compared to other VLBI efforts owing to the identical antennas in the array. With gating, the VLBA, and a growing population of sources useful for calibration, the astrometric precisions achievable with VLBI continue to improve.

Canonical pulsars (CPs) and, to a lesser extent, MSPs display what is known as red spin noise. Red spin noise is likely caused by complex dynamics at the crust-core interfaces or in the magnetospheres of pulsars. It manifests itself as noise in timing residuals with an approximately power-law power spectrum $P(f) \propto f^{-5}$ (more power at lower frequencies, hence the moniker "red") and can be characterized by stochastic shifts in the period or period derivative of a pulsar. The stochasticity of red spin noise

---

[1] Department of Physics
[2] Department of Astronomy

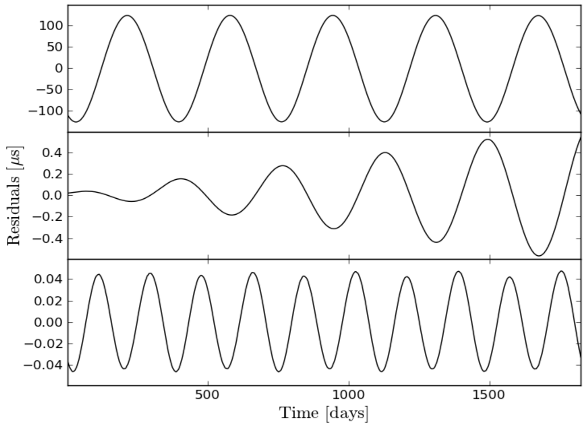

FIG. 1.— The characteristic signature in timing residuals caused by errors in position, proper motion, and parallax (from top to bottom respectively). For a pulsar with the coordinates of PSR 1713+0747, these are the residuals associated with 0.1 arcsecond errors in δ and π and 0.1 arcsecond per year errors in μ_δ. The oscillations in the top two plots have a 1 year period and the oscillations in the bottom plot have a 6 month period. The amplitudes of these curves scale linearly with the errors in the astrometric parameters.

makes it impossible to incorporate into a deterministic timing model. In contrast to white noise, the excess of low frequency power in red spin noise introduces correlations over finite timescales. These correlations give red spin noise a non-trivial shape that can vary substantially from realization to realization.

Along with red spin noise, gravitational waves (GWs) induce structure in timing residuals. There are current efforts to detect the signature of isolated, continuous sources (Lee et al. 2011; Ellis et al. 2012) and burst sources (Finn & Lommen 2010; Pshirkov et al. 2010; van Haasteren & Levin 2010; Cordes & Jenet 2012) of GWs in timing residuals, but among the most promising types of GW signals from an initial detection perspective is that of a stochastic background (SB) created by an ensemble of merging supermassive black holes (SMBHs) in the distant universe. The SB is characterized by strains with an amplitude spectrum $h_c(f) \propto f^{-2/3}$ that manifest as a red process in timing residuals having a power spectrum $P(f) \propto f^{-13/3}$ (Jenet et al. 2006; Sesana et al. 2008; Cordes & Shannon 2012). Since red spin noise and a SB of GWs both have red spectra with similar spectral indices and could be of comparable magnitudes, it is exceedingly difficult to make a detection of this type of GW in the residuals of a single pulsar. Fortunately, Hellings & Downs (1983) predict that a specific pattern of correlations unique to GWs can be observed in the residuals of an array of pulsars in the presence of a SB of GWs. The European Pulsar Timing Array (EPTA; van Haasteren et al. 2011), the Parkes Pulsar Timing Array (PPTA; Yardley et al. 2011), and the North American Nanohertz Observatory for Gravitational Waves (NANOGrav; Demorest et al. 2012) are timing arrays of pulsars and looking for, among other things, the type of correlations in their residuals predicted by Hellings and Downs.

If one is trying to study the red spin noise of a pulsar or is trying to detect GWs with a PTA, the model fitting applied in timing studies may undermine those efforts. From a statistical standpoint, every fit parameter reduces the degrees of freedom in the data set. Furthermore, if one produces an initial timing model with approximately correct parameters, the timing residuals will contain astrophysical information, but will also contain the signatures of errors in the timing model. Errors in each of the timing model parameters leave characteristic signatures in the timing residuals that have associated structures in frequency space. Minimizing the amplitude of the signature of a timing model parameter error indiscriminately removes power from the residuals at the frequencies associated with that particular signature (e.g., Blandford et al. 1984). The power that is removed from the pre-fit residuals is absorbed by the timing model and causes the parameters of the timing model to shift, possibly away from their true values (Ellis et al. 2011).

Because the spin noise intrinsic to many pulsars and a SB of GWs introduce red processes into timing residuals, we investigate the errors induced in the astrometric parameters of a timing model when they are fit to a series of residuals containing red noise power. In so doing, we demonstrate how red processes can be partially absorbed into a timing model and thus attenuated in the residuals. The deleterious effects of model fitting that we demonstrate can be side-stepped if the timing-independent astrometry of VLBI is incorporated into future pulsar timing models.

In Section 2, we discuss astrometry as it pertains to pulsar timing models, and in particular, derive the signatures in timing residuals associated with errors in position, proper motion, and parallax. In Section 3, we describe simulations we conducted to assess the effects of fitting for astrometry in the presence of red processes on the astrometric parameters of a timing model and on the signature of the red process itself. We follow this with a discussion of our results in Section 4. In Section 5, we discuss the real-world feasibility and benefits of incorporating VLBI astrometry into pulsar timing campaigns. In Section 6, we discuss several applications for VLBI astrometry in pulsar science that are not directly tied to gravitational wave detection. Finally, in Section 7, we summarize our results and provide some concluding remarks.

2. ASTROMETRIC TERMS IN TIMING MODELS

In this section, we discuss the roles of position, proper motion, and parallax in the development of timing models. For a more thorough description of this material, see Backer & Hellings (1986) and Edwards et al. (2006). The pulsar position and proper motion principally affect the Roemer delay. The Roemer delay is the delay between the arrival of a pulse at an observatory and the arrival of that pulse at the solar system barycenter (SSB). It can be written as $\Delta_R = -\boldsymbol{r} \cdot \hat{\boldsymbol{R}}_{\boldsymbol{P}}/c$ where $\boldsymbol{r}$ is the vector pointing from the SSB to the geocenter (we consider errors in the topocentric to geocentric transformation to be negligible), and $\hat{\boldsymbol{R}}_{\boldsymbol{P}}$ is the unit vector pointing from the observatory to the pulsar at the time of the observation.

We use equatorial coordinates α and δ (referenced to the geocenter) in all other sections of this paper, but here, we use an ecliptic coordinate system (centered at the SSB) with longitude λ and a latitude β. Let λ increase with the orbital motion of Earth from an x-axis that points from the Earth to the SSB at the vernal equinox. Place the z-axis such that the Earth orbits in a right-handed fashion. Exploiting the relation $\boldsymbol{r} + \boldsymbol{R_P} = \boldsymbol{r_P}$, where $\boldsymbol{r_P}$ is the vector pointing from the SSB to the pulsar, and approximating the orbit of the Earth as circular, we write

$$\boldsymbol{r} = -\hat{x}R\cos(\omega t) - \hat{y}R\sin(\omega t) \quad (1)$$

$$\boldsymbol{r_P} = \hat{x}D\cos\beta\cos\lambda + \hat{y}D\cos\beta\sin\lambda + \hat{z}D\sin\beta \quad (2)$$

$$\begin{aligned}\boldsymbol{R_P} = {} & \hat{x}\left[D\cos\beta\cos\lambda + R\cos(\omega t)\right] + \\ & \hat{y}\left[D\cos\beta\sin\lambda + R\sin(\omega t)\right] + \hat{z}D\sin\beta, \quad (3)\end{aligned}$$

where R is 1 A.U. and ω is $2\pi/(1\text{ yr})$. If the position and proper motion of the pulsar are determined at $t = 0$ and if any acceleration of the pulsar (from motion in a binary, Galactic rotation, etc.) is ignored, the position can be written as $\beta(t) = \beta_0 + \mu_\beta t$ and $\lambda(t) = \lambda_0 + \mu_\lambda t$ where μ_λ and μ_β are the components of the proper motion. By expanding to linear order in the small parameters μ_λ, μ_β, and $\pi \equiv R/D$ and dropping any constant terms, the Roemer delay can be written as

$$\begin{aligned}\Delta_R \approx \frac{R}{c} & \left[\cos\beta_0\cos(\omega t - \lambda_0)\right. \\ & - \mu_\beta t\sin\beta_0\cos(\omega t - \lambda_0) \\ & - \mu_\lambda t\cos\beta_0\sin(\omega t - \lambda_0) \\ & \left. - \frac{\pi}{2}\cos^2\beta_0\cos(2\omega t - 2\lambda_0)\right]. \quad (4)\end{aligned}$$

Errors in the astrometric parameters, assumed small, produce timing variations that are sinusoids with periods of one year and six months (position and parallax, respectively) and a linearly growing sinusoid with a one-year period (proper motion). This is illustrated in Figure 1. The amplitudes of these oscillations scale linearly with the magnitude of the astrometric error. If a set of residuals display structure resembling a superposition of these signatures, fitting the model to the residuals will lead to adjustments of the astrometric parameters of the model.

3. SIMULATIONS OF NOISE-INDUCED ASTROMETRIC ERRORS & RED NOISE ABSORPTION

We simulated three sets of noiseless arrival times for a pulsar with the astrometry, spin frequency, and spin-down rate of PSR J1713+0747. We did so with the "fake" plug-in for TEMPO2 (Hobbs et al. 2006). In the first set of pulse arrival times (Set A) we simulated one TOA every 3 days over a 500 day span while in the second set (Set B) we simulated one TOA every 21 days over a 500 day span. In the final set (Set C) we simulated one TOA every 21 days over a 3,000 day span.

We added noise of different amplitudes and spectral characteristics to the simulated TOAs. We considered red noise with a power spectrum $P(f) \propto f^{-\gamma}$ with spectral indices $\gamma = 0$, 3, and 5. For each γ, we chose 16 amplitudes for the pre-fit RMS of the noise logarithmically spaced between 10 ns and 10 μs. Once combined with a particular realization of noise of a specific spectral type and RMS amplitude, we reprocessed the simulated pulse arrival times with TEMPO2, fitting for the phase (ϕ), spin period (P), spin-down rate ($\dot{P}$), and astrometry. We recorded the RMS of the post-fit residuals along with the astrometric parameters. For each spectral type of noise and each pre-fit noise amplitude, we did this with 100 different realizations of noise.

We calculated the post-fit astrometric errors as follows:

$$\delta\theta = \left[(\alpha - \alpha_{post})^2\cos^2\delta + (\delta - \delta_{post})^2\right]^{1/2} \quad (5)$$

$$\delta\mu = \left[(\mu_\alpha - \mu_{\alpha,post})^2\cos^2\delta + (\mu_\delta - \mu_{\delta,post})^2\right]^{1/2} \quad (6)$$

$$\delta\pi = |\pi - \pi_{post}|. \quad (7)$$

Here, α, δ, μ_α, μ_δ, and π are the astrometric parameters used to simulate the initial TOAs; the quantities with a subscript "*post*" are the post-fit estimates for them.

4. DISCUSSION OF SIMULATION RESULTS

In Figure 2, we show histograms of the factors by which the pre-fit RMS amplitude of the noise are reduced by fitting. For simulation Sets A and B, which correspond to 500 days of observations, significant amounts of red noise are absorbed into the model. In both cases, the redder the noise, the more severe the absorption. In the reddest case, the pre-fit RMS amplitude of the red noise is reduced by a factor of about 20 in the median case. The problem is less severe in the simulations with longer observation spans (Set C). Even so, in the reddest case, the pre-fit levels of red noise can be reduced by up to a factor of five.

Figures 3, 4, and 5 (corresponding to simulations Sets A, B, and C, respectively) show errors in the astrometric parameters of the timing model when they are fit in the presence of noise. In all cases, the noisier the pre-fit residuals, the noisier the post-fit residuals and the bigger the errors in the astrometric parameters. These figures also depict the reduction of the RMS noise level that is caused by fitting. Like in Figure 2, it is apparent that the absorption of red noise is a more severe problem for the 500 day simulations in Sets A and B than it is for Set C; this can be straightforwardly explained. Fitting for phase, period, and period-derivative removes a quadratic from the pre-fit residuals. The post-fit residuals will thus consist of cubic and higher-order contributions. The higher order contributions will be suppressed in red processes that have less power in higher frequencies. A zero-mean polynomial dominated by a cubic contribution can readily mimic a sinusoid with a one year period if the data set has a length of approximately one year. If the data set is significantly longer than one year, this is not such a problem. Similarly, if one has only 6 months of data, quadratic subtraction may leave a shape in the residuals resembling the 6-month-period sinusoid associated with errors in parallax.

In Figures 3, 4, and 5, there is a stark difference between $\gamma = 0$ (white noise) and the $\gamma = 3$ and 5 cases. With white noise, the 100 points associated with each of our 16 levels of input pre-fit RMS noise fall into significantly more compact regions of the plane for position, proper motion, and parallax. These regions are particularly compact in the horizontal dimension. All realizations of white noise are comparably non-covariant with the signatures of astrometric errors in the timing model. On the other hand, some realizations of red noise can be more covariant with the signatures of astrometric errors in the timing model than other realizations. Some realizations of red noise can be more readily attenuated

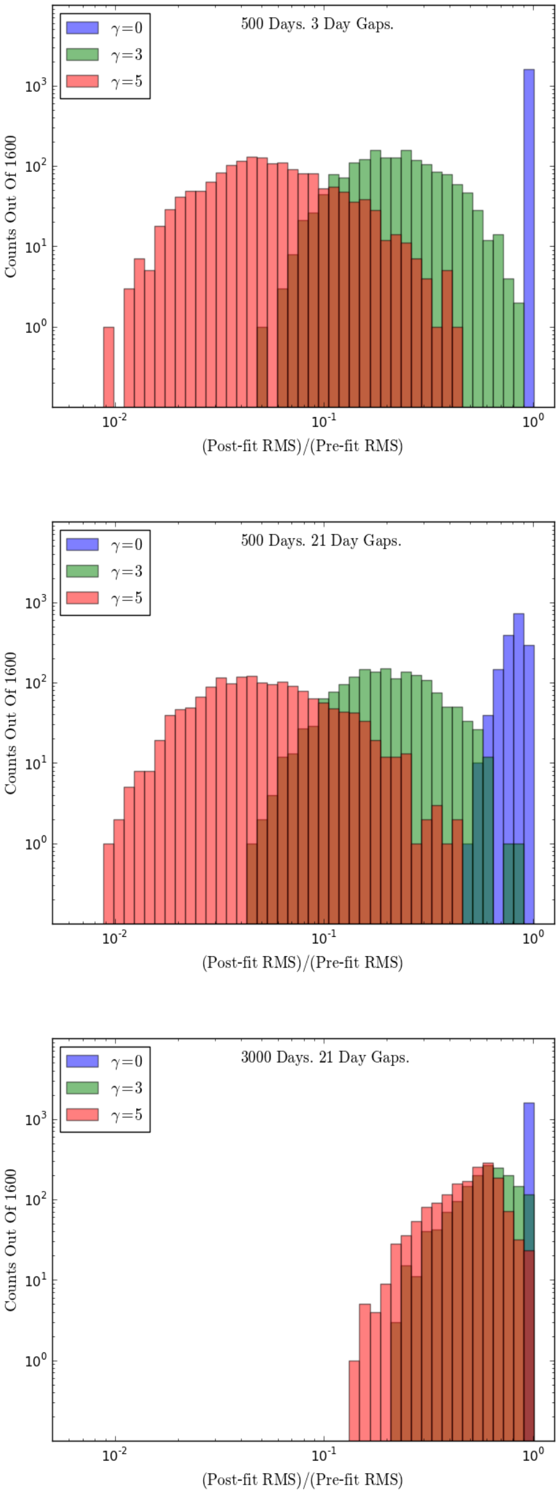

FIG. 2.— Ratios of post-fit RMS to pre-fit RMS for simulated arrival times. Each of the three histograms in each panel corresponds to input noise of a different spectral index (γ = 0,3,5). Each histogram contains 1600 counts for the 100 realizations of noise at each of 16 pre-fit rms amplitudes. Redder noise is more readily absorbed into the astrometric parameters of a timing model, but the amount of absorption is reduced as observation spans grow significantly longer than 1 yr.

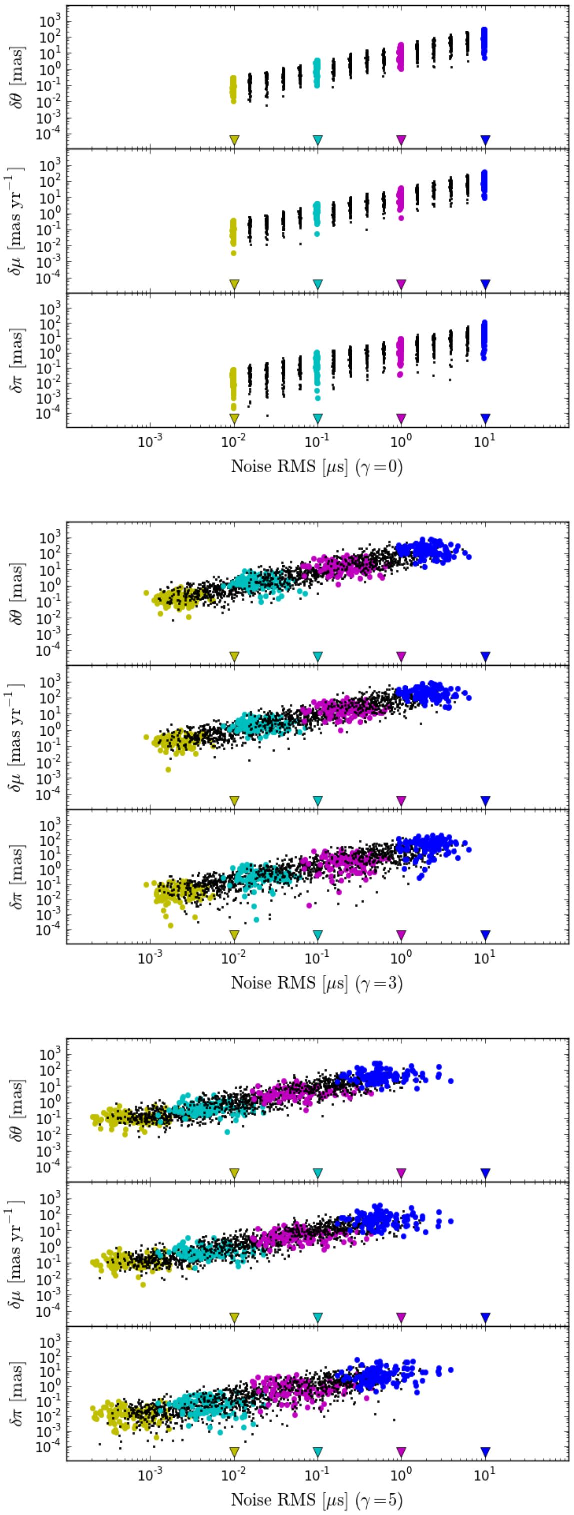

FIG. 3.— Astrometric errors (offset between true astrometric parameters and post-fit estimates of astrometric parameters) versus post-fit RMS for simulation Set A (500 days of TOAs taken at 3 day intervals). The three panels of the three plots each contains 1600 points corresponding to the 100 realizations of noise at 16 input levels of pre-fit noise. Moving downwards through the three plots, the spectral index of the additive noise increases from 0, to 3, to 5. The yellow points correspond to an input pre-fit rms of 0.01 μs (this is indicated by the triangular magenta indicator above 0.01 μs). Similarly, cyan, magenta, and blue points correspond to input pre-fit rms values of 0.1, 1, and 10 μs repsectively. The top, middle, and bottom panel of each plot indicates the noise-induced post-fit error in the position, proper motion, and parallax respectively.

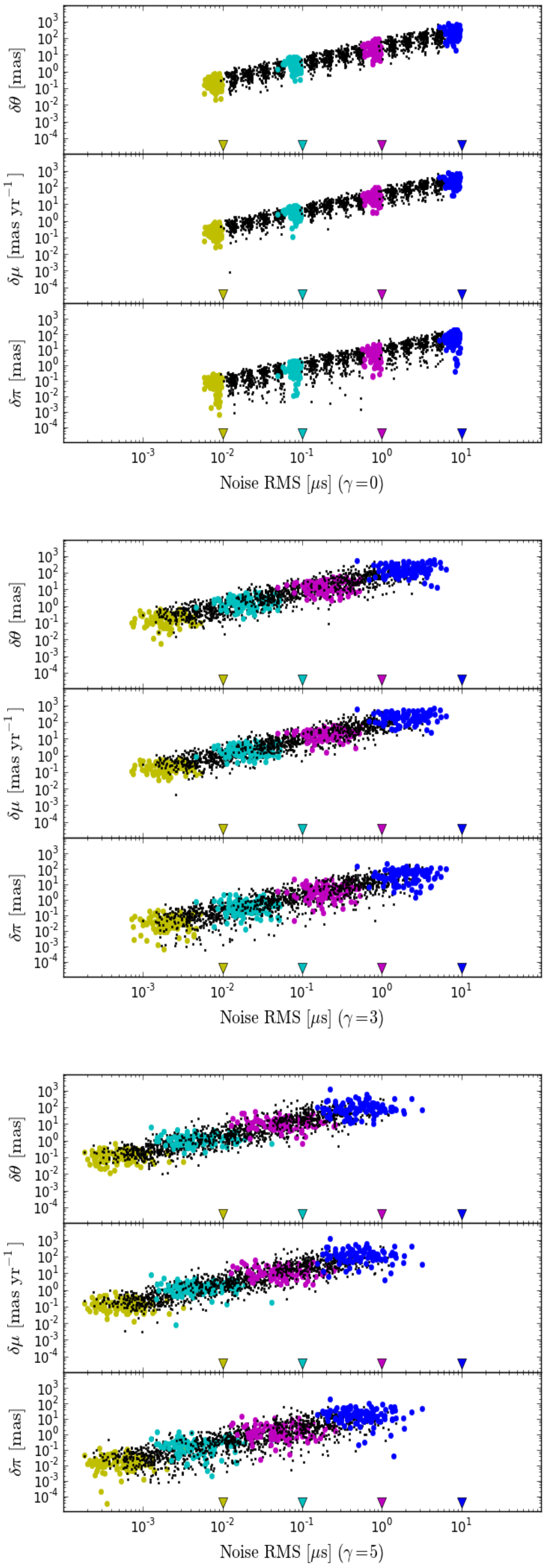

FIG. 4.— As in Figure 3, but for simulation Set B (500 days of TOAs taken at 21 day intervals).

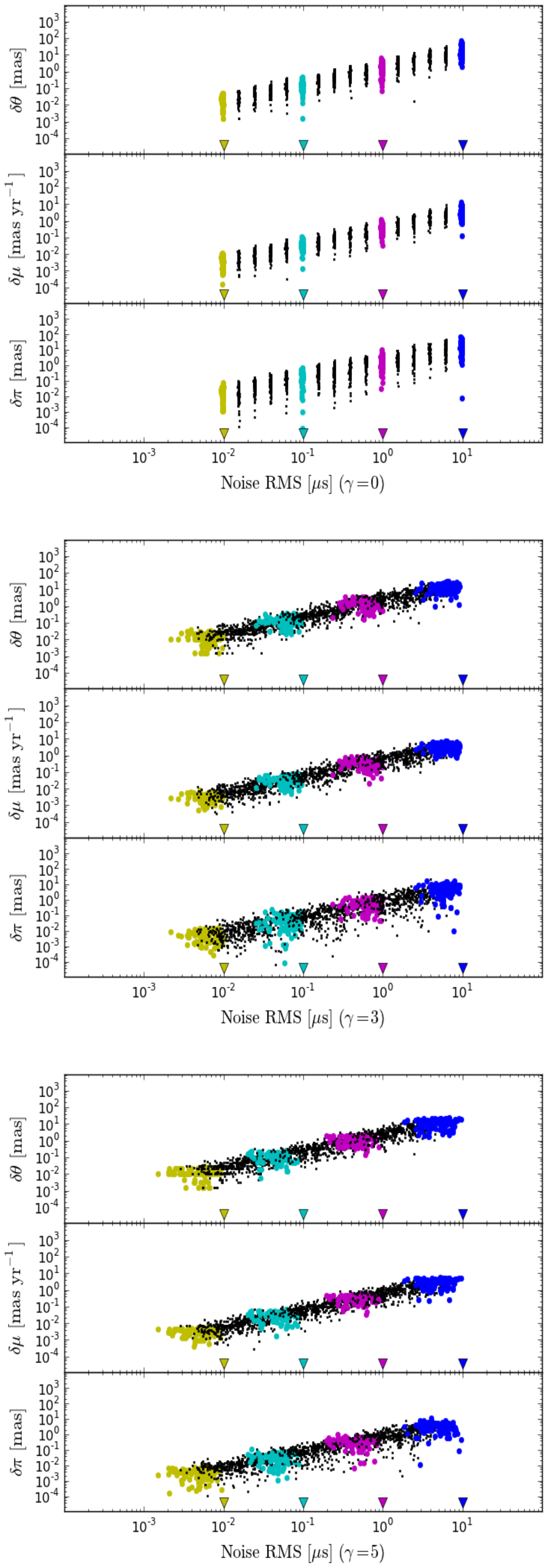

FIG. 5.— As in Figure 3, but for simulation Set C (3000 days of TOAs taken at 21 day intervals).

in post-fit residuals than others by modifying the astrometric parameters of the timing model; this leads to the increased horizontal scatter in simulations involving red noise.

5. INCORPORATING VLBI ASTROMETRY INTO PTAS

Given a sufficient S/N and sufficient calibrators, modern VLBI can provide absolute position estimates relative to the International Celestial Reference Frame (ICRF) to 1 mas precision after 1 year, proper motion estimates to 0.01 mas yr^{-1} precision after 2 years, and parallax to 0.01 mas precision after three years (e.g., Chatterjee et al. 2009). From Figures 3, 4, and 5, we can infer the post-fit RMS noise amplitudes at which noise-induced errors in the astrometric parameters reach levels comparable to the precisions achievable with VLBI. A summary of our conclusions is presented in Table 1. The best-timed pulsars to date have post-fit RMS residuals of several tens of nanoseconds over several year spans (Yardley et al. 2011; van Haasteren et al. 2011; Demorest et al. 2012). In all cases in Table 1 (except for position estimates in our 3000 day simulated data sets), VLBI can provide better astrometric measurments than timing techniques for nearly all known pulsars, even the best-timed ones.

5.1. *Reference Frame Considerations*

Astrometric measurements with VLBI are made relative to the ICRF (Ma et al. 1998), a geocentric, quasi-inertial frame referenced to distant quasars. Pulsar timing is carried out in a dynamic reference frame centered on the SSB and oriented relative to the orbital plane of Earth; this coordinate system is set by a solar system ephemeris such as the Jet Propulsion Laboratory's DE405 (Standish 1998). Position measurements of some pulsars with VLBI and pulsar timing are inconsistent, indicating that the quoted measurement errors are too small. To demonstrate the inconsistency between VLBI and timing-based astrometry, in Table 2, we show VLBI and timing-based position measurements of pulsars J0437−4715 and J1713+0747. The two timing-based position estimates for pulsar J1713+0747 in Table 2 are also inconsistent with one another. This inconsistency is also due, at least in part, to reference frame differences as Splaver et al. (2005) use the DE200 (Standish 1990) solar system ephemeris while Hotan et al. (2006) use the more accurate DE405 ephemeris. Proper motion and parallax measurements are less susceptible to such frame-related offsets as they depend more on the changes in celestial coordinates over time than the absolute coordinates. However, as Eq. 4 demonstrates, timing corrections associated with proper motion and parallax depend on the position of the pulsar, so reference frame mismatch will influence the degree to which VLBI-based and timing-based proper motion and parallax measurements can be made to agree.

By measuring the absolute position of a pulsar with both timing and VLBI at approximately contemporaneous epochs, it is possible to constrain the two-angle rotation needed to transform between the ICRF and the relevant pulsar timing reference frame to milliarcsecond precision or better (e.g., Bartel et al. 1996). If comparably precise VLBI and timing astrometry is measured for N_P pulsars and the measurement errors are uncorrelated from pulsar to pulsar, the errors in the frame transformation can be reduced by a factor $\propto N_P^{-1/2}$. At the outset of a timing campaign on a sample of newly discovered pulsars, pre-existing measurements such as those presented in Table 2 can be used to refine the frame tie to an extent that would allow VLBI astrometry to immediately be used in timing models in place of estimates derived from timing data. With large VLBI astrometry campaigns like the PSRπ project (Deller et al. 2011) currently under way, it is likely that all pulsars in PTAs will soon have VLBI astrometry available. As TOAs are collected, timing models should be refined using standard techniques, but the astrometric parameters of the model will not have to be fitted.

Once the time baseline has significantly exceeded one year, the PTA data can be made independent of the pre-existing frame tie by combining the timing data and the VLBI astrometric measurements and doing one simultaneous, global fit over all pulsars and the frame tie. Using timing residuals from all pulsars in a PTA to constrain the frame-tie parameters will require incorporating currently existing tools like TEMPO2 into a more elaborate framework that can simultaneously fit the timing models of all the pulsars in the array as well as the frame-tie parameters with appropriate weighting to account for different uncertainties. For a PTA with 17 pulsars, Demorest et al. (2012) fitted 1382 parameters. Of these parameters, 1171 dealt with a time-varying dispersion measure or pulse profile evolution across the band. With more thorough multi-frequency observation, many of these parameters will become unnecessary. The remaining frequency-dependent parameters will be determined by features unique to the residuals of individual pulsars and will prove highly non-covariant with parameters that affect the quality of the global fit. Of the remaining 211 parameters, 85 are astrometric parameters that could be provided by VLBI if 2 additional frame-tie parameters are included in the fitting procedure.

5.2. *Incorporating New Pulsars Into PTAs While Utilizing VLBI Astrometry*

Suppose a new MSP is discovered and its timing stability and brightness make it a prime candidate for PTA science. In the first couple of years of observations, if timing and VLBI studies begin concurrently and are combined appropriately, attenuation of the amplitude of red processes in the timing residuals caused by model fitting can be dramatically reduced. To quantify this, we introduce some formalism taken from Blandford et al. (1984). The timing residuals, $R(t)$, are fit to a linear combination of basis functions associated with the parameters being fit for. To simplify matters, consider only eight parameters as follows:

$$R(t) = \sum_{i=1}^{8} \lambda_i \psi_i(t) \tag{8}$$

$$\begin{aligned}
\psi_1(t) &= 1 & \psi_5(t) &= \cos(\omega t)\\
\psi_2(t) &= t & \psi_6(t) &= t\cos(\omega t)\\
\psi_3(t) &= t^2 & \psi_7(t) &= t\sin(\omega t)\\
\psi_4(t) &= \sin(\omega t) & \psi_8(t) &= \sin(2\omega t).
\end{aligned}$$

TABLE 1

NDays (days)	gap (days)	NTOA	γ	A_θ(1 mas) (ns)	A_μ(0.01 mas yr^{-1}) (ns)	A_π(0.01 mas) (ns)
500	3	169	5	< 1	<1	<1
500	3	169	3	< 2	<1	<1
500	3	169	0	35	<10	<10
500	21	25	5	1	< 1	< 1
500	21	25	3	2	< 1	<1
500	21	25	0	8	<10	<10
3000	21	145	5	100	5	2
3000	21	145	3	120	7	3
3000	21	145	0	200	< 10	<10

Note. — Levels of post-fit noise RMS indicative of astrometric errors on par with precisions achievable with VLBI astrometry. Moving from left to right, the first two columns indicate the number of days worth of TOAs and the gap (in days) between TOAs for the set of simulated TOAs used for the simulations associated with that row. The third column is the total number of simulated TOAs in that set. The fourth row indicates the spectral index of the power spectrum of the noise added to the pristine set of TOAs. The last three columns indicate the RMS amplitude of noise in the post-fit residuals at which the noise-induced error in position, proper motion, or parallax is big enough that VLBI would provide more accurate astrometry. If a "less-than" sign is used, the interpretation is that post-fit RMS noise well below that level is indicative of errors bigger than precisions available from VLBI.

TABLE 2

PSR	Measurement Type	$\Delta\alpha$ (s)	$\Delta\delta$ ($''$)	Reference
J0437−4715	VLBI	0.883250(3)	0.031863(37)	Deller et al. (2008)
. . .	Timing	0.883185(6)	0.034033(70)	Verbiest et al. (2008)
J1713+0747	VLBI	0.5306(1)	0.519(2)	Chatterjee et al. (2009)
. . .	Timing 1	0.5307826(7)	0.52339(3)	Splaver et al. (2005)
. . .	Timing 2	0.53077(1)	0.5228(2)	Hotan et al. (2006)

Note. — Astrometric positions measured with VLBI and pulsar timing for PSR J0437−4715 and PSR J1713+0747. For PSR J0437−4715, $\Delta\alpha$ is the offset from right ascension $04^h37^m15^s$ and $\Delta\delta$ is the offset from declination $-47°15'09''$ at MJD epoch 54100. For PSR J1713+0747, $\Delta\alpha$ is the offset from right ascension $17^h13^m49^s$ and $\Delta\delta$ is the offset from declination $07°47'37''$ at MJD epoch 52275.

The basis functions $\psi_i(t)$ are associated with $\phi, P, \dot{P}, \alpha, \delta, \mu_\alpha, \mu_\delta,$ and π respectively. The coefficients λ_i are functions of the true spin and astrometric parameters of the pulsar and the fractional errors in the timing model estimates of them. Assuming N years of observations have been made, the basis functions can be converted to an orthonormal set of basis functions, $\psi'_i(t)$, using the Gram-Schmidt process with the inner product

$$\psi_i(t) \cdot \psi_j(t) = \int_{-N/2}^{N/2} \psi_i(t)\psi_j(t)dt. \tag{9}$$

We then compute the Fourier transform of each basis function, $\tilde{\psi}'_i(f)$, and combine them into a transmission function, $T(f)$ as follows:

$$\tilde{\psi}'_i(f) = \int_{-N/2}^{N/2} \psi'_i(t) \exp{(2\pi\imath f t)} dt \tag{10}$$

$$T(f) = 1 - \frac{1}{N}\sum_{i=1}^{8} \tilde{\psi}'_i(f)\tilde{\psi}'^{*}_i(f). \tag{11}$$

If the structure in the pre-fit timing residuals is due entirely to some process with a stationary power spectrum $P(f)$, the mean-square post-fit residual coming from frequencies between f_L and f_H is given by

$$\bar{R^2} = \int_{f_L}^{f_H} T(f)P(f)df. \tag{12}$$

The transmission function is a filter on the pre-fit variance and dictates what fraction of power in the pre-fit residuals at a particular frequency makes it through the fitting procedure and into the post-fit residuals.

If sufficiently precise VLBI astrometry is available and reference frame mismatches have been dealt with, certain parameters do not need to be fit for. The process described above can be repeated with any subset of the basis functions listed in Eq. 8. We assume that after the first year of timing and VLBI observations, VLBI estimates for position are precise enough that they do not need to be fit for. After 2 years, the VLBI estimates for proper motion reach sufficient precision, and after 3 years, VLBI can determine parallax well enough that no astrometric fitting is necessary. In Figure 6, we demonstrate how the transmission function varies in the first 5 years of observation if VLBI astrometry is or is not incorporated into timing efforts according to this schedule.

The sensitivity enhancements when VLBI astrometry is used are apparent in Figure 6. Using VLBI astrome-

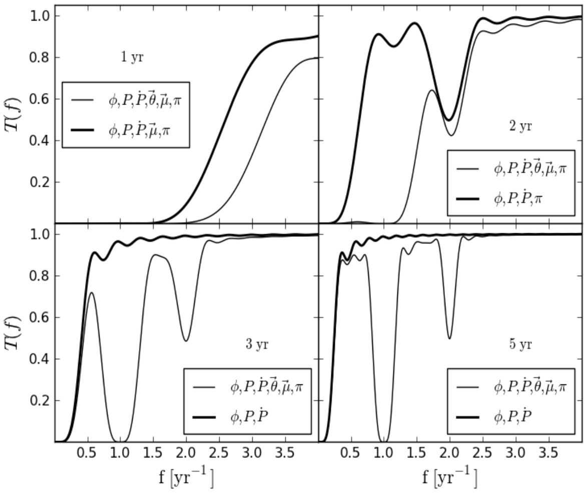

FIG. 6.— Transmission functions for 1, 2, 3, and 5 year data sets with and without using astrometric measurements from VLBI. The legends indicate the spin and astrometric parameters being fit to produce the associated transmission function. In the 5 year transmission function in which all 8 parameters are fit, the prominent absorption feature at the origin ($f = 0$ yr^{-1}) is associated with the quadratic fit to the spin parameters of the pulsar, the feature at 1 yr^{-1} is associated with fitting out the oscillations associated with errors in position and proper motion, and the feature at 2 yr^{-1} is associated with fitting out parallax errors.

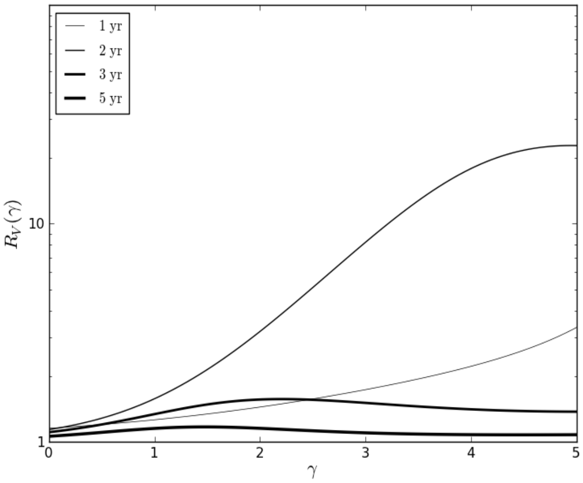

FIG. 7.— The ratio of post-fit residual variance using VLBI astrometry to that without using VLBI astrometry versus the spectral index of a red process in the TOAs. Each curve is associated with one panel from Figure 6, as is indicated by the legend. It is assumed that astrometric parameters from VLBI are incorporated into the timing model according to the same schedule used to make Figure 6; after 1 year, VLBI provides $\boldsymbol{\theta}$, after 2 years, it also provides $\boldsymbol{\mu}$, and at the 3 and 5 year marks, VLBI is providing all 5 astrometric parameters. The quantity being plotted is R_V from Eq. 13.

try, it will be possible to detect coherent sources of GWs with frequencies of approximately 1 yr^{-1}, a prospect that is entirely hopeless without VLBI. Aside from this very specific type of source, because the bulk of the sensitivity enhancement occurs at low frequencies (below about 3 yr^{-1}), the sensitivity of PTAs to red processes could be greatly enhanced. To quantify the enhancement to red process sensitivity, for a range of spectral indices γ, we compute the following variance ratio:

$$R_V(\gamma) = \frac{\int_{f_L}^{f_H} T_{VLBI}(f) f^{-\gamma} df}{\int_{f_L}^{f_H} T(f) f^{-\gamma} df} \tag{13}$$

where $T_{VLBI}(f)$ is the transmission function when VLBI astrometry is used and $T(f)$ is the transmission function when all the astrometry is fit for. We set the low frequency cutoff $f_L = 0$. The low-frequency absorption feature common to all the transmission functions in Figure 6 approaches zero as f^6 for small f, so each of the integrals in Eq. 13 will converge for $\gamma < 7$. We set the high frequency cutoff $f_H = 9$ yr^{-1} corresponding to the Nyquist frequency if 18 equispaced measurements are made each year. The results of this calculation are shown in Figure 7. As γ increases (steeper power spectrum), the increased amplitude of the transmission function at low frequencies when VLBI information is used becomes increasingly important so as to not filter out substantial amounts of the power through fitting. The enhanced sensitivity is most pronounced after two years with red processes having a spectral index very near 13/3, the value expected from a SB of GWs. The enhancement can be greater than a factor of 20 in this case. This is consistent with our findings from Figure 2 that for data sets 500 days in length, red noise with a spectral index of 5 is attenuated by fitting by a factor of 20 in the median case. Once the data set becomes longer than three years, the transmission functions with and without VLBI astrometry differ only by the prominent absorption features at 1 and 2 yr^{-1}. The width of these features Δf is approximately proportional to f/N so the feature at $f = 1$ yr^{-1} has a width $\Delta f \approx N^{-1}$ yr^{-1} and the feature at $f = 2$ yr^{-1} has a width $\Delta f \approx 2N^{-1}$ yr^{-1}.

6. ADDITIONAL VLBI AND TIMING SYNERGIES

So far, we have emphasized the significance VLBI astrometry can have in PTA efforts to detect GWs. Here, we briefly discuss additional types of pulsar timing science that could be aided by VLBI astrometry.

6.1. *Relativistic Evolution of NS-NS Binaries*

Pulsars in compact binaries show post-Keplerian (PK) evolution described by parameters that include the rate of periastron advance, the gravitational redshift, and the rate of orbital period decay. Within any theory of gravity, these PK parameters are functions of the unknown masses of the two objects in the system and the measurable Keplerian parameters. Measurements of any two independent PK parameters yield estimates of the two masses. Measurements of additional PK parameters provide tests of that theory of gravity (Stairs 2003). Studies of the binary systems PSR B1913+16 (Hulse & Taylor 1975; Weisberg et al. 2010) and PSRs J0737−3039A/B (Kramer et al. 2006) have in this way provided stringent tests of general relativity (GR) and, through measurements of the rate of orbital period decay, $\dot{P}_b$, the best indirect evidence for gravitational radiation to date.

Measurements of $\dot{P}_b$ are complicated by the fact that, in the timing model, a decaying orbital period is covariant with the relative acceleration of the centers of mass of the compact binary and the SSB. Additionally, the Shklovskii effect is an apparent relative acceleration caused by a changing line of sight to the pulsar that depends on the proper motion and distance to the pulsar as $\mu^2 D$ (Shklovskii 1969). For some binaries, like PSR B1534+12, the Shklovskii effect can be the dominant bias preventing an accurate measurement of $\dot{P}_b$ (Stairs 2003). If the proper motion and parallax of a pulsar are provided by VLBI, the bias can be removed (Deller et al. 2009a).

For B1913+16, despite the existence of over 30 years of timing data, VLBI estimates of the astrometric parameters will be of higher precision than those derived from timing. Pulsars in NS-NS binaries have larger magnetic fields than MSPs and therefore are expected to have greater spin noise (e.g., Shannon & Cordes 2010). Over approximately 30 years, B1913+16 has timing residuals with an RMS of $\sim$100 μs and there was a glitch in the rotational frequency of the pulsar in 2003 with $\Delta f/f \approx 3.7 \times 10^{-11}$ (the glitch is indicative of red spin noise in B1913+16 at some level). Despite decades of observations, Weisberg et al. (2010) derive a timing-based absolute position measurement for B1913+16 with $\sim$1 mas error. Figure 5 shows that even with over eight years of timing data, residuals with an RMS of just 10 μs are indicative of substantial errors in timing-based estimates of the astrometric parameters (10 mas errors in absolute position). Position measurements from VLBI that can reach 1 mas precisions in just one year and are independent of the timing stability of a pulsar provide an improvement over the timing-based position estimates for pulsars in NS-NS binaries. For example, Deller et al. (2009a) combine VLBI astrometry from the Australian Long Baseline Array and timing data for the double pulsar (J0737$-$3039A/B) and find that in the future, with a decade of timing data, measurements of $\dot{P}_b$ for this system will allow a test of GR to 0.01%.

6.2. *Multi-frequency Studies of Newly Discovered γ-ray MSPs*

Recent years have seen an explosion in the population of known MSPs. This is due, in no small part, to the Large Area Telescope (LAT) on the Fermi Gamma-ray Space Telescope. Ray et al. (2012) describe radio follow-ups of a number of LAT pulsar candidates. Of 300 candidates that were γ-ray sources having spectra characteristic of pulsars and signs of variability but no definitive source classification, 47 new pulsars were discovered, 43 of which were MSPs. In one case, by conducting a radio follow-up with the Nançay Radio Telescope on an unidentified LAT γ-ray source, Guillemot et al. (2012) discovered the MSP J2043+1711. Using an ephemeris based on timing data from Arecibo, Nançay, and Westerbork, the γ-ray data were folded and pulsations were detected in the γ-ray band. Additional follow-up observations with Suzaku and the Swift X-ray Telescope failed to identify any X-ray counterpart to J2043+1711.

Given the rapid rate of discovery of MSPs by instruments like LAT, timing observations are limited by the availability of telescope time. VLBI astrometry will accelerate and improve multi-wavelength studies of objects like J2043+1711. The γ-ray sources from LAT are localized to about 1°. If a telescope like the Green Bank Telescope can detect a radio pulsar counterpart to a γ-ray source, the localization will improve to a few arcminutes. At this point, standard pulsar timing techniques can be used to develop a timing model that will allow for, e.g., the detection of pulsations in γ-rays for J2043+1711 (Guillemot et al. 2012). But, until several years of timing data are collected, timing will be unable to constrain the position of the pulsar sufficiently to allow successful identification of a unique X-ray counterpart. Furthermore, there is a chance that a newly discovered pulsar may exhibit high levels of timing noise that substantially skews timing-based astrometric estimates. After the pulsar is localized to within a few arcminutes by an initial radio detection, we can instead use interferometry (e.g. with the Very Large Array and then VLBI) to constrain the position to milliarcsecond precisions. Efforts to detect the pulsar in X-rays can be better guided and unique X-ray counterparts can be picked out. Rapid, high-precision astrometry from VLBI will facilitate efforts like that of Guillemot et al. (2012) and will aid studies of the pulsar across the entire electromagnetic spectrum.

7. CONCLUSIONS

Standard model fitting procedures used in pulsar timing can falter in the presence of red processes. Whether from red spin noise or the activity of a SB of GWs, fitting the timing model by minimizing the RMS of the residuals causes the power in the red process to be absorbed into the timing model at the cost of shifting the timing model parameters to erroneous values.

VLBI provides an alternative means of measuring the astrometric parameters of a pulsar with sufficiently high precision that these measurements can be adopted by timing models without fitting. We find that for even the best-timed pulsars to date, if standard model fitting is employed on data sets not significantly longer than 1 year, the noise-induced errors in the astrometric parameters can exceed the precisions achievable with VLBI in similar time spans. Furthermore, by incorporating VLBI astrometry into timing models for newly discovered pulsars, after collecting data for just two years, the power present in post-fit residuals from red processes having spectral indices characteristic of a SB of GWs can be enhanced by a factor of 20. VLBI can additionally be used to aid multi-wavelength studies of the rapidly growing population of MSPs; characterizing and monitoring these new MSPs will help to grow PTAs and thus aid in GW detection.

For known pulsars with decades of timing data, VLBI astrometry has an advantageous but less significant influence on the timing. It dramatically enhances the chances of detecting coherent GW signals with periods of six months or a year. Aside from this small class of GW sources, using VLBI astrometry will only boost the signal of a $\gamma = 13/3$ red process by about 2% in ten years of timing data. The reduction in the number of parameters being fitted in a timing model is a permanent improvement for χ^2 tests for the presence of signal in the data, but this becomes less significant as more TOAs are collected and the number of degrees of freedom in the data grows. For some of the most well studied pulsars, those in relativistic binaries, even those having decades of timing data, VLBI astrometry will be of higher precision than timing astrometry and will allow correction for the Shklovskii effect to improve measurements of the PK parameters of these systems. The decrease in the number of timing model parameters being fit for and the ability to augment the power of a SB of GWs in the timing residuals of a pulsar in certain cases by a factor as substantial as 20 may play a key role in the initial direct detection by PTAs of GWs.

We thank A. Deller, G. Hobbs, M. McLaughlin, S. Ransom, J. Lazio, and other members of the NANOGrav and PPTA collaborations for much helpful discussion. We thank P. Demorest and, again, G. Hobbs for answering many questions regarding TEMPO2. This work was supported by a subaward to Cornell University from West Virginia University from NSR/PIRE Grant 0968296. S. Chatterjee also acknowledges support from the NASA Fermi mission through the grant NNX11AO34G.

REFERENCES

Backer, D. C., & Hellings, R. W. 1986, ARA&A, 24, 537
Bartel, N., Chandler, J. F., Ratner, M. I., et al. 1996, AJ, 112, 1690
Blandford, R., Romani, R. W., & Narayan, R. 1984, Journal of Astrophysics and Astronomy, 5, 369
Chatterjee, S., Brisken, W. F., Vlemmings, W. H. T., et al. 2009, ApJ, 698, 250
Cordes, J. M., & Chernoff, D. F. 1997, ApJ, 482, 971
Cordes, J. M., & Jenet, F. A. 2012, ApJ, 752, 54
Cordes, J. M., & Lazio, T. J. W. 2002, arXiv:astro-ph/0207156
Cordes, J. M., & Shannon, R. M. 2012, ApJ, 750, 89
Deller, A. T., Bailes, M., & Tingay, S. J. 2009a, Science, 323, 1327
Deller, A. T., Tingay, S. J., Bailes, M., & Reynolds, J. E. 2009b, ApJ, 701, 1243
Deller, A. T., Verbiest, J. P. W., Tingay, S. J., & Bailes, M. 2008, ApJ, 685, L67
Deller, A. T., Brisken, W. F., Chatterjee, S., et al. 2011, arXiv:1110.1979
Demorest, P. B., Ferdman, R. D., Gonzalez, M. E., et al. 2012, arXiv:1201.6641
Edwards, R. T., Hobbs, G. B., & Manchester, R. N. 2006, MNRAS, 372, 1549
Ellis, J. A., Jenet, F. A., & McLaughlin, M. A. 2012, ApJ, 753, 96
Ellis, J. A., McLaughlin, M. A., & Verbiest, J. P. W. 2011, MNRAS, 417, 2318
Faucher-Giguere, C. ., & Kaspi, V. M. 2007, arXiv:0710.4518
Finn, L. S., & Lommen, A. N. 2010, ApJ, 718, 1400
Guillemot, L., Freire, P. C. C., Cognard, I., et al. 2012, MNRAS, 422, 1294
Hellings, R. W., & Downs, G. S. 1983, ApJ, 265, L39
Hobbs, G. B., Edwards, R. T., & Manchester, R. N. 2006, MNRAS, 369, 655
Hotan, A. W., Bailes, M., & Ord, S. M. 2006, MNRAS, 369, 1502
Hulse, R. A., & Taylor, J. H. 1975, ApJ, 195, L51
Jenet, F. A., Hobbs, G. B., van Straten, W., et al. 2006, ApJ, 653, 1571
Kramer, M., Stairs, I. H., Manchester, R. N., et al. 2006, Science, 314, 97
Lee, K. J., Wex, N., Kramer, M., et al. 2011, MNRAS, 414, 3251
Lorimer, D., & Kramer, M. 2005, Handbook of Pulsar Astronomy (Cambridge : Cambridge University Press)
Ma, C., Arias, E. F., Eubanks, T. M., et al. 1998, AJ, 116, 516
Manchester, R. N., & Taylor, J. H. 1977, Pulsars (San Francisco : W. H. Freeman)
Pshirkov, M. S., Baskaran, D., & Postnov, K. A. 2010, MNRAS, 402, 417
Ray, P. S., Abdo, A. A., Parent, D., et al. 2012, arXiv:1205.3089
Sesana, A., Vecchio, A., & Colacino, C. N. 2008, MNRAS, 390, 192
Shannon, R. M., & Cordes, J. M. 2010, ApJ, 725, 1607
Shklovskii, I. S. 1969, AZh, 46, 715
Splaver, E. M., Nice, D. J., Stairs, I. H., Lommen, A. N., & Backer, D. C. 2005, ApJ, 620, 405
Stairs, I. H. 2003, Living Reviews in Relativity, 6
Standish, Jr., E. M. 1990, A&A, 233, 252
—. 1998, JPL IOM 312.F-98-048
Toscano, M., Sandhu, J. S., Bailes, M., et al. 1999, MNRAS, 307, 925
van Haasteren, R., & Levin, Y. 2010, MNRAS, 401, 2372
van Haasteren, R., Levin, Y., Janssen, G. H., et al. 2011, MNRAS, 414, 3117
Verbiest, J. P. W., Bailes, M., van Straten, W., et al. 2008, ApJ, 679, 675
Weisberg, J. M., Nice, D. J., & Taylor, J. H. 2010, ApJ, 722, 1030
Yardley, D. R. B., Coles, W. A., Hobbs, G. B., et al. 2011, MNRAS, 414, 1777